A Multiphysics Finite Element Model of a 35A Automotive Connector Including Multiscale Rough Surface Contact

Santosh V. Angadi

Robert L. Jackson[1]
e-mail: robert.jackson@eng.auburn.edu

Song-yul Choe

George T. Flowers

Center for Advanced Vehicle and Extreme Environment Electronics,
Department of Mechanical Engineering,
Auburn University, Auburn, AL 36849

Bong-Yi Lee

Liang Zhong

LS Cable Company, Ltd.,
Anyang, Gyeonggi-do,
431-080 South Korea

Electrical contacts influence the reliability and performance of relays, electrical connectors, high power connectors, and similar systems, and are therefore a key region which needs to be considered. In the current study, a new inclusive multiphysics (involving mechanical, electrical, and thermal fields) finite element model (FEM) of a 35A automotive connector has been developed. The contact resistance is predicted using a multiscale rough surface contact method and is embedded in the multiphysics FEM. The coupled connector model is solved to obtain stresses, displacements, contact pressures, electrical and thermal contact resistances, voltage, current density, and temperature distributions. It appears that the current flows mostly through very small regions that are usually near the contacting surfaces in the connector, thereby suggesting that the available conducting material can be more efficiently used by developing optimized connector designs. Through analytical calculations and experimental measurements of temperature rise (ΔT or change in temperature) for the cable and the connector, it is believed that a large portion of the temperature rise in actual 35A connectors is due to the Joule heating in the supply cables. The model is a powerful tool that can be used for the basic connector characterization, prototype evaluation, and design through various material properties, and surface finishes. [DOI: 10.1115/1.4005955]

Keywords: automotive connector, multiphysics, multiscale rough surface contact, modeling

1 Introduction

Hybrid and electrical vehicles (HEVs) appear to be the next evolutionary step of the automobile. However, the electrical systems which propel HEVs are fundamentally different from conventional automobile technologies. HEVs comprise of many new technologies and so there is limited information on their life and reliability. Connectors are also an important and critical component of any vehicle containing electrical components. Connectors in HEVs are known to carry very high currents (high power) [1] and due to this there can be a tremendous increase in temperature in these parts during service. High power and the automotive environment (high temperature, vibrations, humidity, etc.) can cause degradation and failure of the connectors. If the connector contacts degrade, the contact resistance can increase and cause other problems with the power electronics and controls of the electrical power drive system. Eventually, connectors could catastrophically fail and become either permanently welded together or effectively nonconductive.

At higher magnifications, it is evident that an electrical contact or any engineering surface possesses roughness when viewed on a microscopic scale although it appears smooth on a macroscopic scale. In reality, when two surfaces come in contact with each other, they are in contact through the asperities or peaks on their surfaces [2]. This implies that there is a reduced real area of contact between two contacting surfaces. The load is carried by the asperities on the contacting surfaces. Due to the relatively high load being carried by the isolated asperities, they usually deform in an elasto-plastic manner. A smaller real area of contact causes constriction for the flow of electric current and conduction of heat between the surfaces (Fig. 1). This constriction phenomena together with poorly conducting impurities present on the surfaces (for example, oxides) leads to electrical contact resistance (ECR) and thermal contact resistance (TCR). However, in the case of TCR, due to gaps (Fig. 1) between the contacting surfaces, the heat transfer may also occur through convection. Electrical current may also flow across thin films due to electron tunneling [3–5]. However, in the current work these mechanisms are considered relatively insignificant and are neglected.

There are many different methods to model the contact of rough surfaces including statistical [6–10], fractal [11–15], and multiscale models [16–18]. Kogut and Etsion performed an earlier analysis of electrical connectors while considering elastic deformation of a curved beam or connector spring and the elastic–plastic deformation of the surface asperities [19]. However, they used a statistical rough surface contact model that does not consider multiple scales of roughness. Their model also does not include the multiphysical effects such as Joule heating and thermal expansion that are considered by the current methodology.

The fractal mathematics based methods were derived to account for the different scales of surface features not accounted for by the statistical models [11–15]. The most common fractal contact methodology assumes that the surfaces can be described by the self-affine Weierstrass-Mandelbrot fractal. However, it has been shown that using this self-affine fractal to describe surfaces also results in an unphysical prediction of zero contact area [17,20,21]. The multiscale models were developed to alleviate the assumption of self-affinity imposed by fractal mathematics and to also improve how the mechanics are considered.

The idea of multiscale contact was first developed by Archard [22] by considering the elastic contact of stacked spheres. Other works in the literature on the multiscale rough surface contact include Ciavarella and Demelio [23] and Persson [24]. Jackson

[1]Corresponding author.

Contributed by the Electronic and Photonic Packaging Division of ASME for publication in the JOURNAL OF ELECTRONIC PACKAGING. Manuscript received April 30, 2010; final manuscript received January 19, 2012; published online March 7, 2012. Assoc. Editor: Shidong Li.

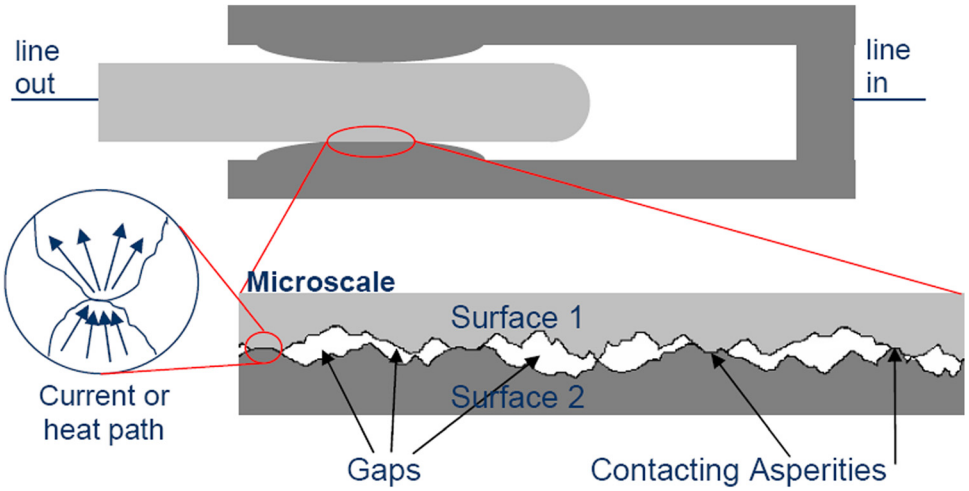

Fig. 1 Schematic representation of current and heat flow in 35A connector

and Streator [18] developed this model further by using data from a Fourier transform of the surface profile to describe the asperity scales (see Fig. 2). The model takes into account many scales of roughness via stacking. In this model, a large asperity is modeled to have many asperities of smaller size on it. Each of these smaller asperities again contains several very small sized asperities and so on.

Several articles have been published in the literature related to the modeling of electrical contacts in connectors [25–28]. Electrical contacts are critical regions in relays, switches, connectors, and similar systems. When subjected to a high number of cycles or long term usage, the contacts may get damaged and are prone to failure. Also, through the fretting corrosion process, the degradation of the electrical contacts is primarily caused by vibration of the connectors and the resulting relative motion between the contacting surfaces.

In the current investigation, a multiphysics finite element model of a 35A rated connector that also considers multiscale rough surface contact at the contacting surfaces is developed. The multiphysics 35A connector model serves as a comprehensive and powerful tool to increase the fundamental understanding of the behavior of high power connectors by taking into account the coupled mechanical, electric, and thermal phenomena seen in connectors (this will be discussed in greater detail later).

Also, the model includes the coupled effects of nanoscale to macroscale surface roughness, applied current, electric potential (voltage drop), Joule heating, and thermal expansion. This cutting edge model provides a prediction of the contact forces, ECR, TCR, current density, stresses, displacements, and temperature in the bulk regions of the connector parts. In this work, micro and nanoscale roughness were included through the multiscale rough surface contact model [29] (executed prior to the multiphysics FEM connector model to obtain contact resistance predictions). The multiphysics connector model is not refined enough to include micro and nanoscale roughness deterministically as the mesh would need an unrealistic amount of refinement on the surface.

Since the multiscale rough surface contact model is only executed before the FEM model initiates, it is different than a previous multiphysics connector model [25]. Nonetheless, the authors are not aware of any peer-reviewed journal publication on the methodology or results of a multiphysics model of an electrical connector. In addition, in the previous work [25] only a generic connector geometry with one set of contacting surfaces was considered, while in the current work a more realistic connector geometry is considered that includes three sets of contacting surfaces. Actually, the additional sets of contact surfaces caused convergence problems when the previous methodology [25] was used. An updated version of the multiscale contact resistance model is also used in the current work [21]. Hence, a new methodology is developed.

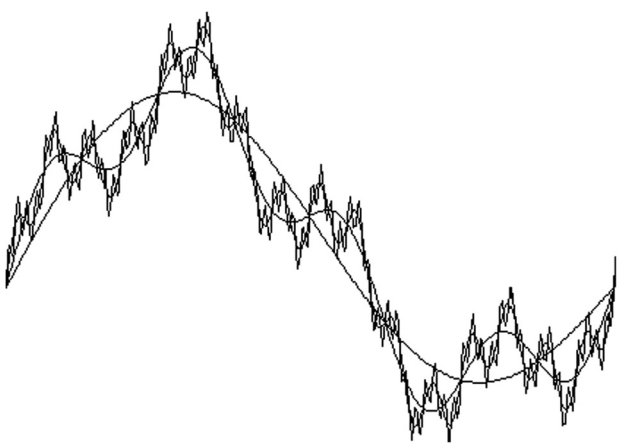

Fig. 2 Schematic depicting the decomposition of a surface into superimposed sine waves. Each line represents a different scale of roughness.

2 Modeling Methodology

The model solves the mechanical–electric–thermal coupled fields of equations (see Fig. 3) and thus captures effects not normally considered by conventional uncoupled finite element models. In Fig. 3, E is the elastic modulus, ν is the Poisson's ratio, σ is the normal stress, τ is the shear stress, ε is the normal strain, γ is the shear strain, I is the electrical current, Φ is the electrical potential across the connector, ρ is the electrical resistivity, k is the thermal conductivity, T is the temperature distribution, Q is the heat flux, α is the thermal expansion coefficient, and ΔT is the change in temperature of the material. For instance, the heat generated in the connector will be due to Joule heating (Q_{joule}). This heating will increase the temperature (T) which will cause thermal expansion ($\alpha\Delta T$) and stresses (σ, τ) in the connector parts. This deformation will change the geometry and in turn redirect the flow of electrical current and heat.

The mechanical field of the problem considers the stresses (σ, τ) and strains (ε, γ) of the material, and how it will deform and possibly fail due to over stressing. The theory of elasticity is used to model the deformations in the material. Then, three dimensional Hooke's law, which relates the stresses and strains via the

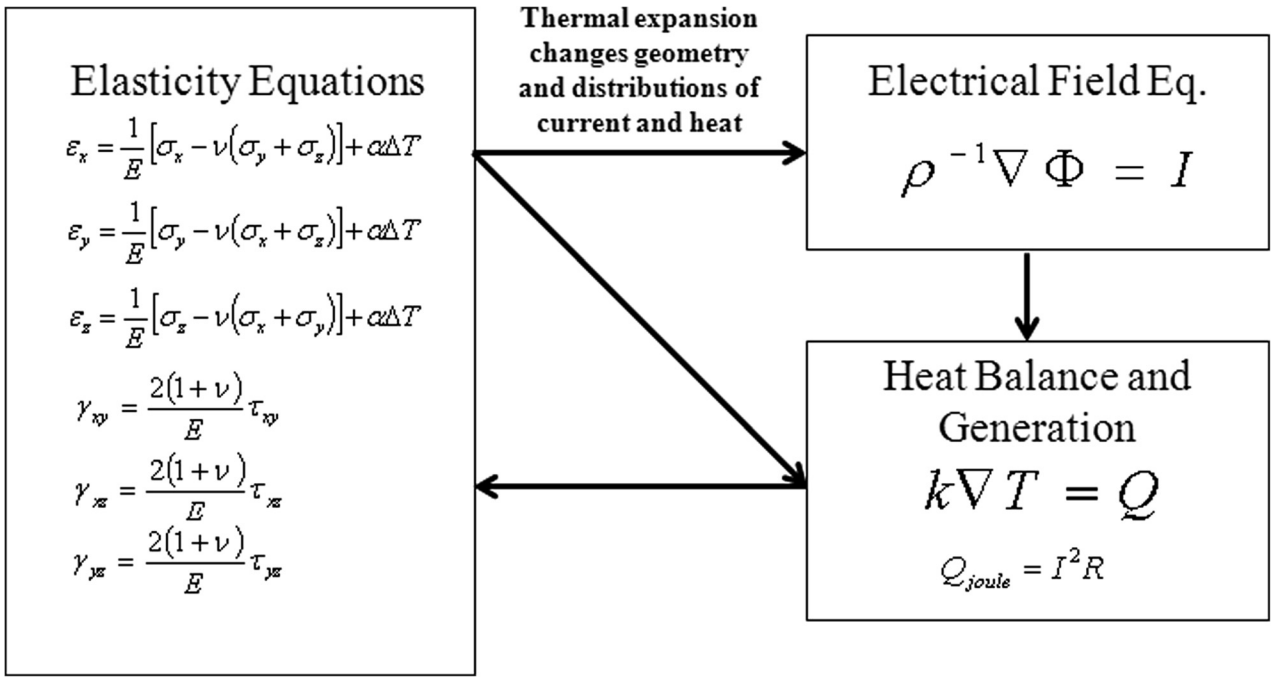

Fig. 3 Schematic showing the coupled multiphysics field equations

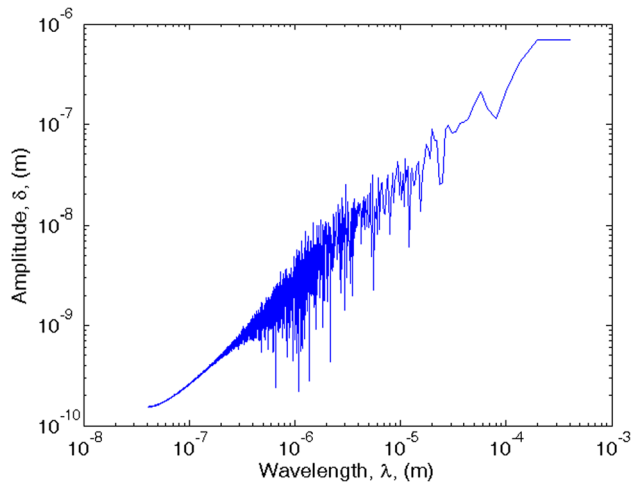

Fig. 4 Fourier series of connector surface showing asperity amplitude as a function of scale

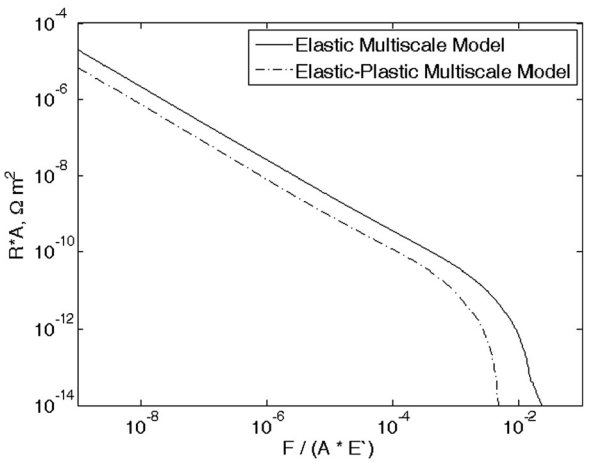

Fig. 5 The ECR values predicted from the multiscale models to be used in the multiphysics connector model

elastic modulus (E) and Poisson's ratio (υ), is given in Cartesian coordinates (x,y,z), as shown in Fig. 3.

The thermal and electrical fields are coupled, and the mechanical and thermal fields are coupled. For the prescribed connector geometry and boundary conditions, the multiphysics ANSYS™ software (version 11) solves these equations simultaneously for more realistic predictions.

ECR and TCR values are predicted using the multiscale model [21] from a micro and nanoscale profile of the connector surface. A stylus profilometer is used to obtain rough surface data for contacting surfaces of 35A connector. A fast Fourier transform of the surface is taken and the complex conjugate of each term is found, resulting in the predicted surface asperity amplitudes versus scale shown in Fig. 4. The resulting ECR values as a function of normalized average contact pressure are given in Fig. 5. ECR predictions considering only elastic contact and elastic–plastic contact are shown, although only the elastic–plastic results are used in the full connector model. As expected, the elastic–plastic ECR values are lower than the elastic ECR values because the model predicts more area of contact between the surfaces. For the elastic–plastic predictions, a yield strength of 41 MPa was used to model the tin plated surfaces, in addition to the properties in Table 1. Note that the ECR values can be easily converted to thermal contact resistance values by substituting the thermal conductance for the electrical conductance.

In our earlier work [25], the mechanical, thermal, and electrical contact interaction of the parts of the electrical connector are modeled by the multiscale rough surface contact method using an external code that iteratively communicates with ANSYS™. However, in this work, a new method that employs only ANSYS™ to reach convergence is established to solve the multiphysics finite element and multiscale rough surface contact based model [21] of the connectors. This new method is simpler and enables faster convergence. Thus, there is no need for an external code to run simultaneously with ANSYS™.

We have solved problems of simple constant cross section wires conducting electricity with heating and thermal expansion

Table 1 Material properties for spring and pin parts of the 35A connector

Material property	Copper based alloy material (bulk material)	Tin material (surface finish material)
Modulus of elasticity (N/mm^2)	137×10^3	41.4×10^3
Poisson's ratio	0.32	0.33
Coefficient of thermal expansion (K^{-1})	17.1×10^{-6}	23.8×10^{-6}
Electrical resistivity (Ω mm)	2.05×10^{-5}	11.5×10^{-5}
Thermal conductivity (W/mm K)	316×10^{-3}	63.2×10^{-3}

and compared them to analytical solutions, but they are not included in this work as they are very fundamental and simple in nature. We have also produced other results for models of situations such as solenoid valves which consist of a long coil of wire that heats significantly and also compared the results to experiments [30,31].

Generally, electrical connectors are made up of two main parts, namely, the spring and the pin. The shape of the spring resembles a curved beam and is compliant, whereas the pin is flat. The main function of the spring is to provide a sufficient contact force between the two parts. The geometry of the spring and pin parts of the 35A connector model are shown in isometric form in Fig. 6. Since the cross section of the connector varies little, except at the sidewalls, a simplified 2D model of the connector has been developed in the current work. A cross section of the 35A connector aligning with one of the two indentation features (see Fig. 6) in 2D is taken and is modeled in ANSYS™. The resulting cross section is shown in Fig. 8. The dimensions of the model geometry in ANSYS™ are in millimeters.

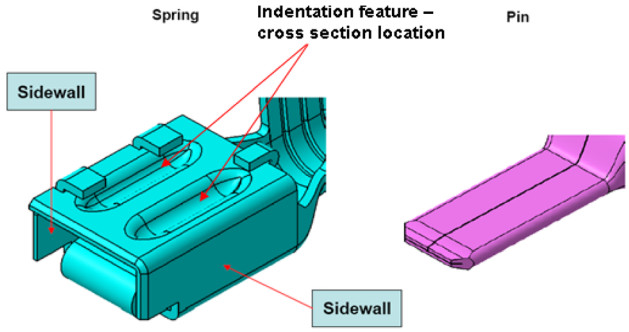

Fig. 6 35A connector model parts (for modeling analysis)

Several simplifying assumptions have been made in the model:

(1) The bulk connector model assumes the plane stress assumption.
(2) In the current model, the connector is assumed to be perfectly elastic (multiscale rough surface contact is still considered elastic–plastic).
(3) Only the steady-state solution to the problem is considered (i.e., the current and the temperature do not vary with time).
(4) Convection/conduction from the outer surfaces of the connector parts is neglected because the properties of the plastic connector casing are considered to be a good insulator relative to the metal components.

The total number of elements (including PLANE223 and LINK68 elements) used in the model are 7828. PLANE223 element is a two dimensional eight node direct-coupled (structural–electric–thermal) element. The LINK68 element is a uniaxial coupled thermal–electric element for electrical and thermal conduction between contacting points.

At first, the multiscale rough surface contact model is used to predict the contact resistances as a function of contact pressure. The 35A connector geometry is set up in ANSYS™. The material properties of the copper based alloy material used to manufacture the bulk of the 35A connector are assigned in ANSYS™ (see Table 1). However, a tin material is used to plate the surfaces of the 35A connector and those properties are also given in Table 1. The properties of the plating were only used in the multiscale model to predict the contact resistances as a function of contact pressure resulting from the micro and nanoscale rough surface profile. The properties of the bulk material were only used in the FEM model of the macroscale connector. Notice that thermal expansion is currently not considered in the multiscale contact resistance model and so the property is not required.

The element types are then set. The various paths of current and heat flow are indicated in Fig. 7. The mesh is shown in Fig. 8. Additionally, both the spring and pin parts are meshed uniformly so that they will contact near the nodes on the opposing surface. Then, all the structural, electrical, and thermal boundary conditions are applied (see Fig. 8). The model is adequately constrained structurally in both the x and y directions. The electrical and thermal boundary conditions are applied suitably in the pin and spring parts of the connector such that the current and heat flow, occurring in a real connector during its operation, are simulated. In this

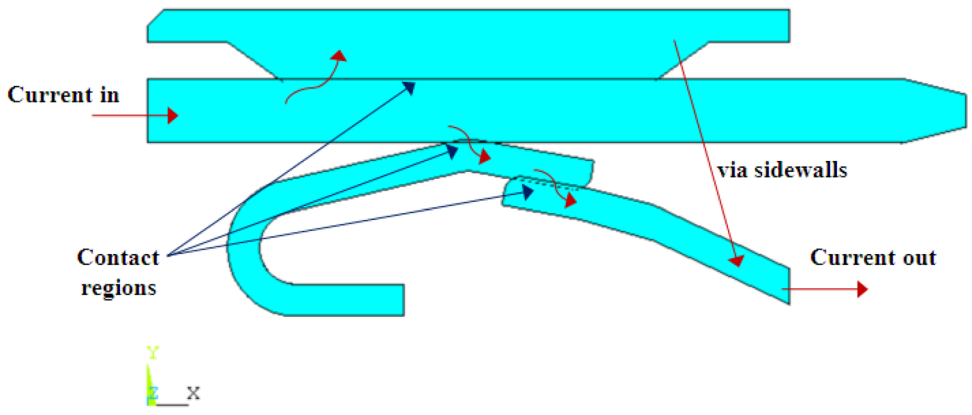

Fig. 7 General current and heat flow directions in the 35A connector model. The actual flow distribution from FEM may be different and more complex three contact regions are also shown.

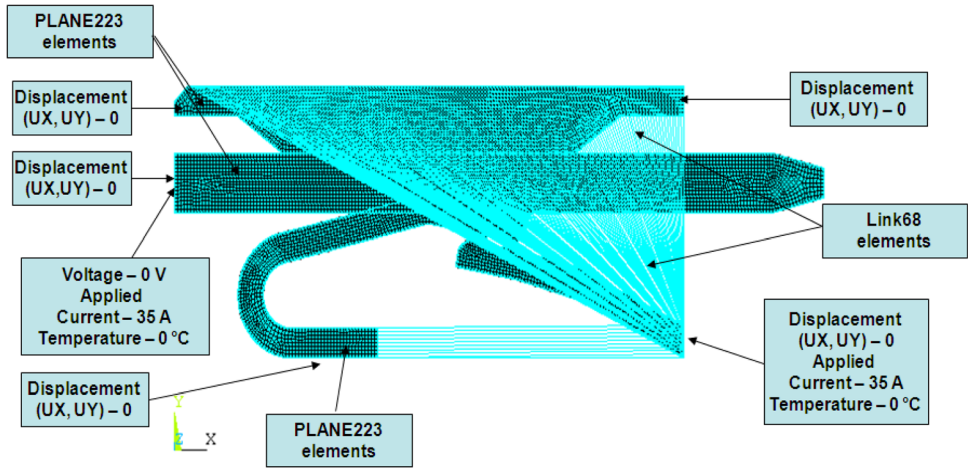

Fig. 8 Boundary conditions for the 35A connector model

method, the 1D Link68 elements are placed to model the conduction of electric current and heat of the sidewalls of the spring terminal of the 35A connector (see Fig. 8).

A critical parameter called thermal deformation (δ), given by Eq. (1), was included to mimic the thermal expansion of the top and bottom surfaces of the sidewalls of the spring terminal of the connector in the ANSYS™ model. In reality, due to the heating of the connector, the sidewalls of the spring terminal of the connector will undergo thermal deformation (δ), that is, thermal expansion

$$\delta = \alpha \times \Delta Ta \times L \tag{1}$$

where α is the coefficient of thermal expansion (/°C), ΔTa is the change in temperature (°C), and L is the original height of the sidewall (mm).

ΔTa is calculated from Eq. (2), which is given by

$$\Delta Ta = \mathrm{T1} - \mathrm{RT} \tag{2}$$

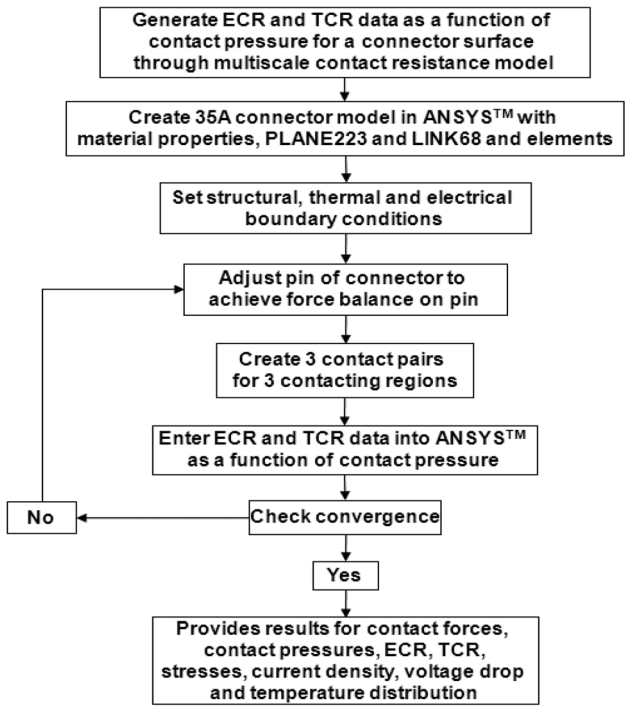

Fig. 9 Flow chart of the 35A connector model

where T1 is the connector temperature at base (°C) obtained from the experiment (see Sec. 4) and RT is the room temperature (22 °C).

To illustrate this, a sample calculation of δ is now provided for one of the applied currents (35 A). For 35 A of current, T1 is 47.63 °C. So, ΔTa equals 25.63 °C. Now, on substituting this value of ΔTa into Eq. (1), we get δ to be 0.001577 mm. However, this δ value is divided by 2, which yields $\delta/2$ as 0.000789 mm. This $\delta/2$ displacement value is then applied separately to each of the top-most and bottom-most surfaces of the sidewalls of the spring terminal. In this way, a total displacement (thermal deformation) of δ (0.001577 mm) is taken into account, which will help to obtain convergence in the 35A connector ANSYS™ model.

Contact pressure, ECR, TCR, thermal, and electrical contact conductance calculations are performed externally before ANSYS™ is executed. To calculate the TCR from the ECR predicted by the multiscale model, the following equation (Eq. (3)) is used:

$$\mathrm{TCR} = \frac{\mathrm{ECR}}{\rho \times k} \tag{3}$$

where ECR is the electrical contact resistance (Ω), ρ is the electrical resistivity (Ω mm), and k is the thermal conductivity (W/mm K).

The contact pairs for the contact regions (see Fig. 7) are created using the contact element (CONTA172) and the target element (TARGE169) for the 35A connector model. During the contact pair creation, the thermal and electrical contact resistance values as a function of contact pressure are read into ANSYS™ from external files. ANSYS™ then uses interpolation to solve for specific values of ECR and TCR as a function of contact pressure.

Initially, the above 35A connector model is run in ANSYS™ with no applied current to enhance convergence. After achieving this convergence, the results of the model without applied current are used as an initial state and the same model is run with application of 35 A current so that complete convergence, involving structural, thermal, and electric fields, is reached for the 35A connector. This helps the solution to converge, which can be very difficult to achieve with a coupled multiphysics model in some cases. Finally, we obtain the displacements, stresses, contact pressures, contact resistances, temperature, electric potential, current density, and Joule heat distributions. A flow chart outlining the sequence of steps for solving the 35A connector model is shown in Fig. 9.

As a check of the reasonableness of the results, after the convergence of the solution was achieved, the force balance on the pin

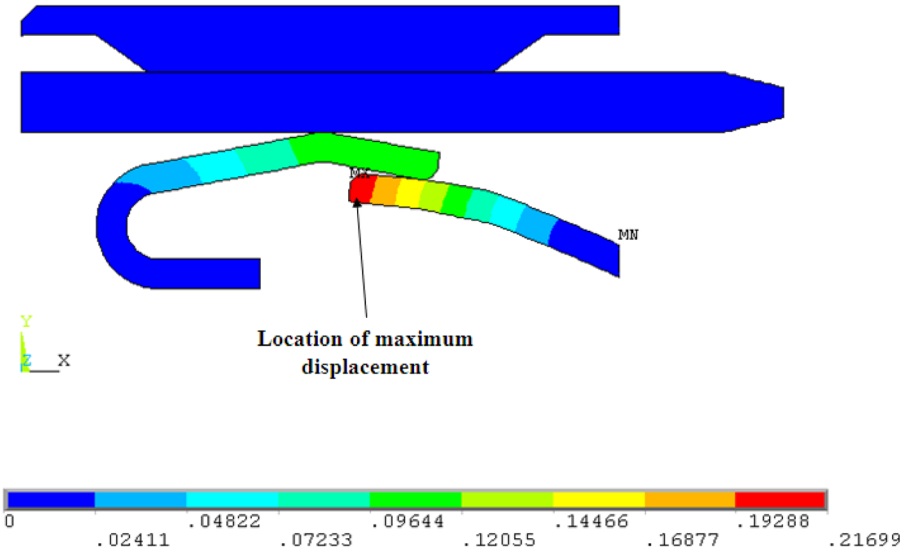

Fig. 10 Displacement (mm) in the 35A connector

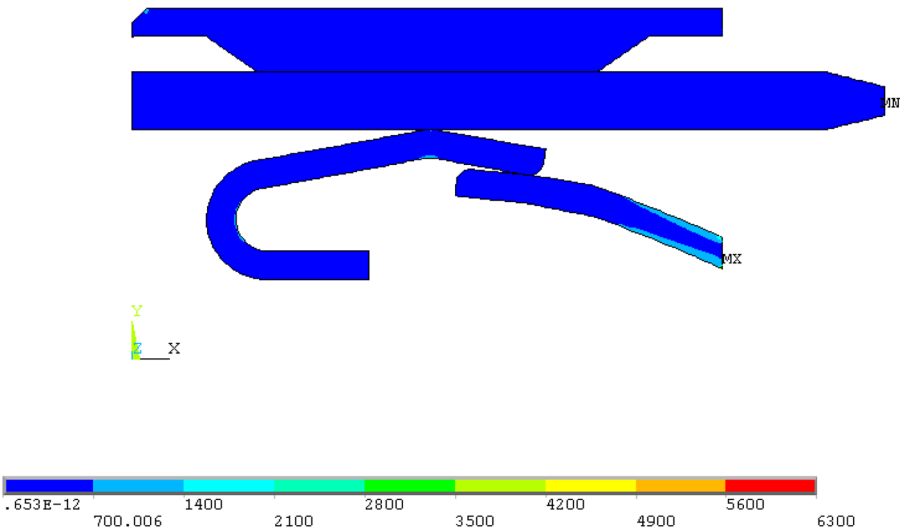

Fig. 11 von Mises stress distribution (N/mm^2) in the 35A connector

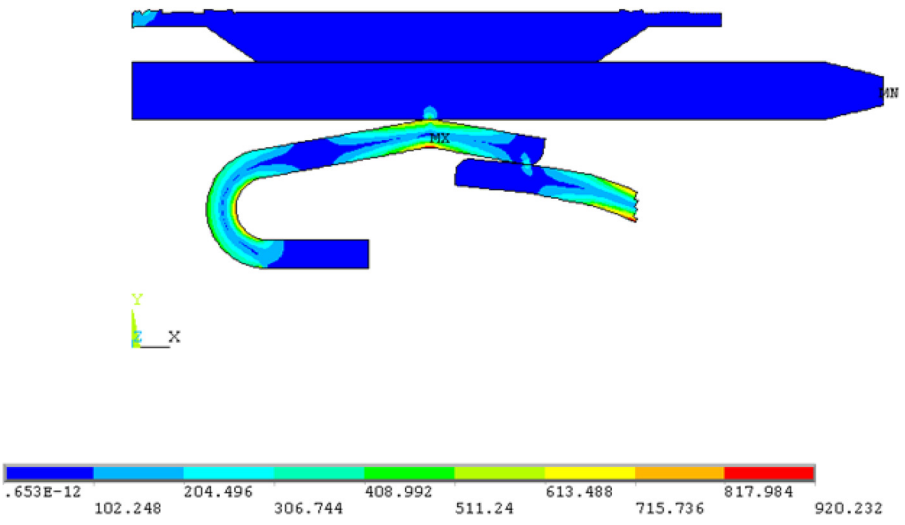

Fig. 12 von Mises stress distribution (N/mm^2) in critical regions of the 35A connector

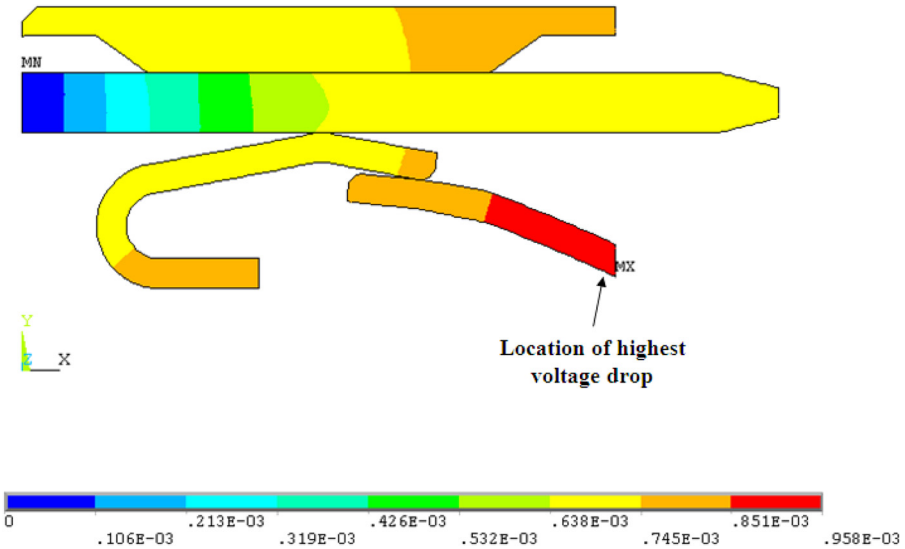

Fig. 13 Electric potential distribution (V) in the 35A connector

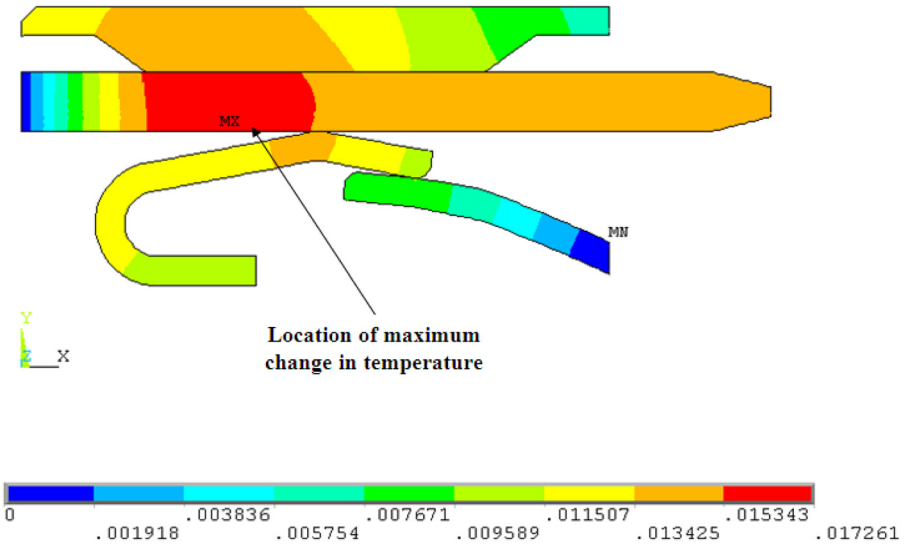

Fig. 14 Temperature distribution (°C) in the 35A connector

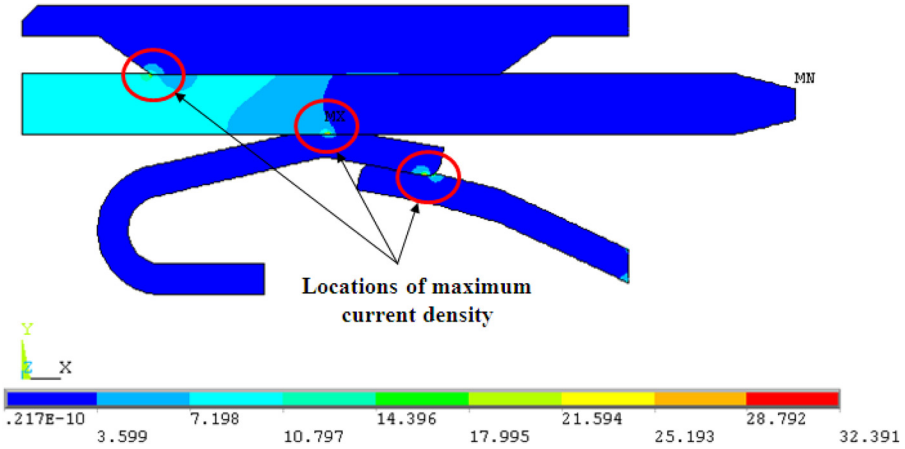

Fig. 15 Conduction current density distribution (A/mm^2) in the 35A connector

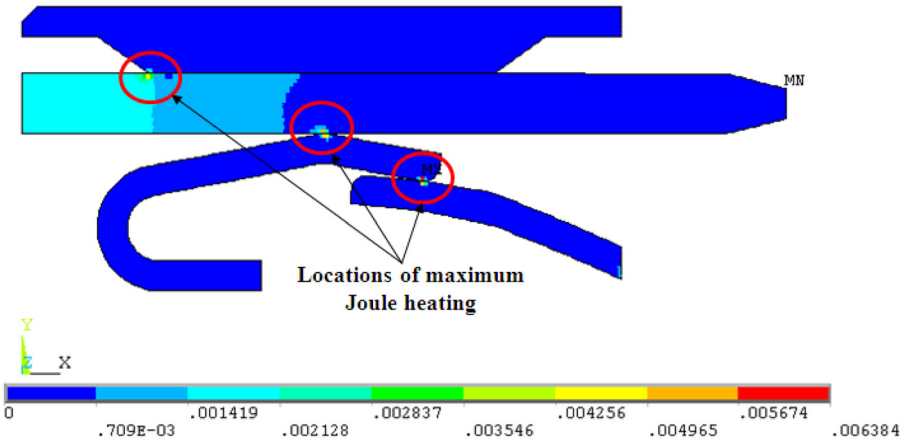

Fig. 16 Joule heat generation per unit volume (W/mm^3) in the 35A connector

terminal of the 35A connector was achieved for an applied current of 35 A in the model. That is, when all the reaction forces in the "Y" direction (Fy) corresponding to all the nodes on the left most end of the pin terminal are summed together, the total value of Fy reaction forces obtained is 1.2026 N. This means that the entire 35A connector model (geometry) within ANSYS™ is practically in an equilibrium state.

3 Results and Discussion

For an applied current of 35 A in the connector model in ANSYS™, the displacement (Fig. 10), von Mises stress (Figs. 11 and 12), electric potential (Fig. 13), temperature (Fig. 14), conduction current density (Fig. 15) distributions, and Joule heat generation (Fig. 16) in the form of contour plots are obtained.

Figure 10 shows the displacement (vector sum) contour plot. Most of the displacement occurs in the bulk regions of the spring terminal that are bent. These bulk regions are the only regions in the entire connector system that can be displaced or adjusted upward or downward to allow the pin terminal to slide in and out of the connector (see Fig. 10). Maximum deformation (displacement), expectedly, is seen at the end of the spring terminal of the connector (as indicated in the above figure) and this portion of the spring is free to move up and down or bend. Also, minimum displacement appears at the right most fixed end of the spring (see Fig. 10) that is constrained in both x and y directions (see Fig. 8) in the ANSYS™ model and in reality, this region of the spring cannot undergo any displacement.

The von Mises stress distribution for the entire connector system is shown in Fig. 11. However, due to high bending stresses in the spring of the connector on the far right, it is difficult to see the stress distribution in the rest of the connector. After removing a portion of the spring, as in Fig. 12, the distribution of the von Mises stress and the critical regions are much more apparent. The maximum von Mises stress locations are marked by "MX" in Figs. 11 and 12. From Fig. 12, it can be noticed that there are also high stresses near the concentrated contacts of the pin and springs and also where the springs are bending (near the curved regions). However, it should be noted that the stresses in the local contacts could actually be higher due to the limited mesh resolution and smaller scale asperity contacts not considered. The predicted maximum von Mises stress value of 6300 N/mm^2 in the bending portion of the spring (Fig. 11) and 920 N/mm^2 in the bend below one of the contacts (Fig. 12) indicates that yielding is probably occurring in the connector because it is higher than the yield strength (for the copper alloy material used in the connector, the yield strength is 540 N/mm^2). Therefore, future versions of connector models should probably be improved to include elastic–plastic material deformation at the macroscale, but were not included here because of the difficulty in obtaining solution convergence.

Figure 13 shows the predicted potential drop between the ends of the connector with the maximum potential being at the spring end and the minimum being at the pin end based on the applied electrical boundary conditions. The potential drop variation is more rapid in the region of the pin terminal that corresponds to concentrated or higher current density (see Fig. 15). Likewise, in the region where there is very low current density, the voltage variation is not as abrupt.

As expected, as shown in Fig. 14, higher temperature gradients (although lower in magnitude) are seen in the pin terminal and in regions where most of the current flows (that is, at the regions where there is higher current density). Temperature rise in the bulk material is not very high. However, experimental measurement of the temperature suggests that it is much higher, and it is therefore believed that this temperature rise is due to the Joule heating in the supplying cables (which are long in length). This issue is explored and explained in more detail in Sec. 5. However, theoretically local asperity temperature should be very high at the contact. Higher temperatures may appear at the microscale level when multiscale rough surface contact is considered at the contacting regions of the connector.

The maximum current density and hence higher temperatures are seen at the contact of spring and pin (Fig. 15). Current density may be used to predict local asperity temperature analytically, but these are not simple calculations to make and there is currently no universally accepted method to do so. Most of the current is concentrated toward the left part of the connector indicating that the current follows the path of least resistance. There are clear concentrated regions of current near the contacting surfaces of the connector. It appears that the current does not distribute itself

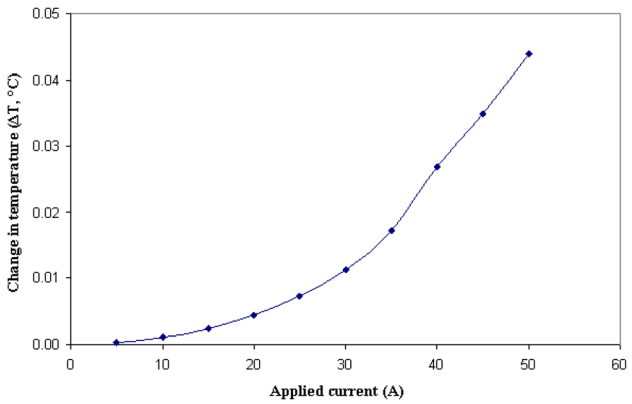

Fig. 17 Effect of increase in current on the change in temperature in the 35A connector

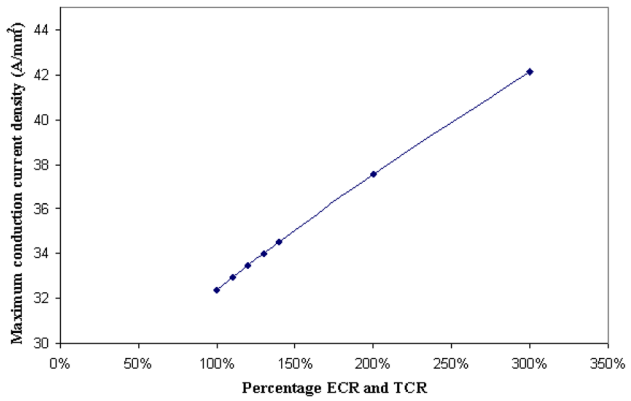

Fig. 18 The effect of an increase in contact resistance on the maximum conduction current density in the 35A connector

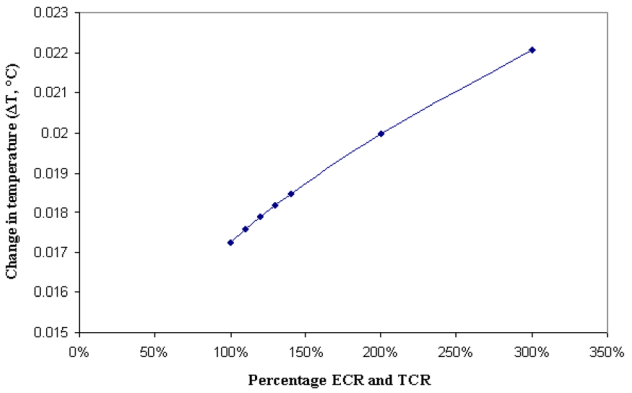

Fig. 19 The effect of an increase in contact resistance on the change in temperature in the 35A connector

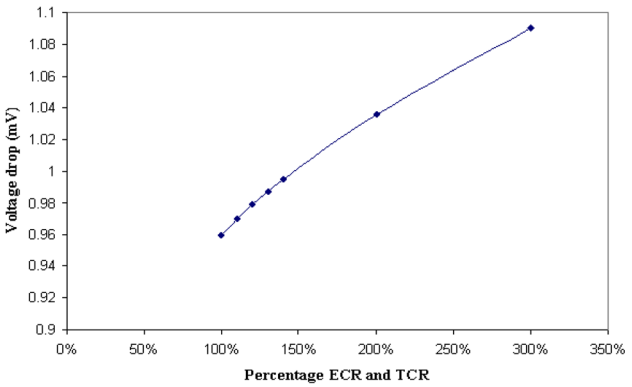

Fig. 20 The effect of an increase in contact resistance on the voltage drop in the 35A connector

evenly across the contact regions and instead tends to flow through very small spots. Maximum current density may be reduced by redesigning the connector so that current is distributed more evenly in the connector.

Figure 16 shows the Joule heat generation contour plot. It shows that Joule heating occurs in the regions where high current density is seen. Again, maximum Joule heating, as expected, appears in the region where current density (Fig. 15) as well as temperature (Fig. 14) is higher. Joule heating is described by Eq. (4) as

$$Q_{\text{joule}} = I^2 R \tag{4}$$

where Q_{joule} is the Joule heat generation, I is the electrical current, and ρ is the electrical resistivity. Again, at the asperity scale it is expected that very high temperatures could arise.

In Fig. 17, it can be noticed that the change in temperature (ΔT or temperature rise) varies with respect to the applied current in a nonlinear (nearly parabolic) way owing to Joule heating in the connector (Eq. (4)). A similar trend was also noticed in an earlier modeling effort on a different electrical connector for the change in temperature versus applied current [25]. This suggests that there is consistency in the trend observed for the 35A connector investigated in this work and the one studied by Angadi et al [25]. Again, the ΔT values for various applied currents in the model are very small. However, the experimental ΔT values are considerably high. Thus, it has been theorized and proved that the Joule heating occurring in the long supply cables causes the high temperature rise (see Sec. 5).

While maintaining a constant applied current of 35 A, the contact resistances (both ECR and TCR) are increased by 10%, 20%, 30%, 40%, 100%, and 200% artificially to predict the possible effect of fretting and surface degradation on parameters such as maximum conduction current density (Fig. 18), change in temperature (Fig. 19), and voltage drop (Fig. 20). As expected, all these three parameters exhibit an increase in their respective values as a result of an increase in contact resistance. Note that both ECR and TCR were increased by the same proportions.

As the contact resistance is increased, the current flow in the connector is more concentrated or more bottlenecked which causes current density to be increased, as shown in Fig. 18. This is not an obvious finding since intuition would suggest that the maximum current density would increase proportionally to the average current density. This could cause the local asperity temperature to be much higher and to cause surface softening and failure where the current density is highest.

From Fig. 19, it can be seen that due to an increase in contact resistance, the change in temperature (temperature rise or ΔT) in the connector increases almost linearly. However, the bulk temperature rise is still relatively small, which indicates that the local temperature rise and temperature rise due to cable heating are much more important. Experimental measurements have shown that during testing the temperature of the connector increases by several more orders of magnitude, but this is believed to be due to heating of the long cables rather than connector heating due to contact resistance (see Sec. 5).

Following Ohm's Law ($V = I\,R$), with a constant applied current, an increase in contact resistance leads to a corresponding increase in the voltage drop across the connector in a nearly linear way (Fig. 20) although there is some nonlinearity to the curve. Therefore, the total resistance of the connector is also increased.

4 Comparison of Simulation and Experimental Results

Equation (5) clearly highlights the relationship between connector resistance (R), ECR and the bulk resistance (bulk_{res}) in the component

$$R = \text{ECR} + \text{bulk}_{\text{res}} \tag{5}$$

A single Sorensen DCS-125E power supply is required to provide the dc for the 35A connectors. The maximum current output of this power supply is 125 A. The analog signals of voltage drop and transmitted current are collected by analog input modules. The temperature readings are collected by thermocouple input modules. The modules are installed in a data acquisition board.

Connector resistance is indirectly estimated by measuring the voltage drop across the connector and dc in the power loop and then by applying Ohm's law: $R = V/I$. The current going through the connector is measured by a LEM IT 400-S current transmitter. This device is able to transduce current into an analog signal with

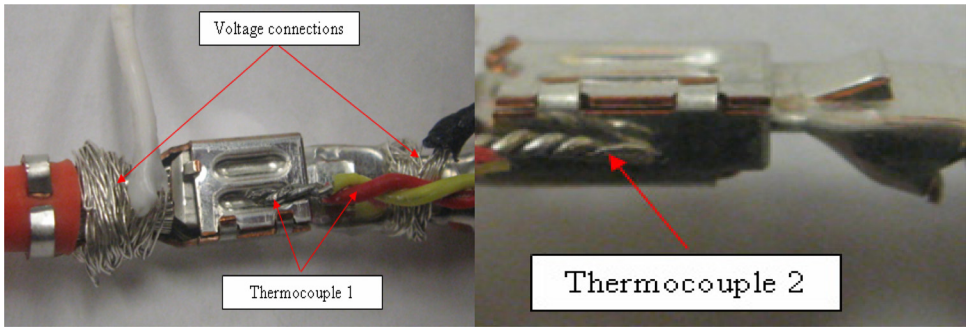

Fig. 21 The placement of thermocouples and voltage measuring wires

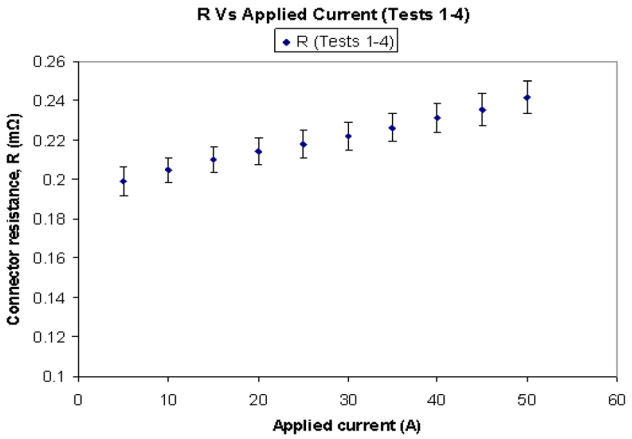

Fig. 22 Connector resistance (*R*) versus constant current in the 35A connector (with error bars for all four tests)

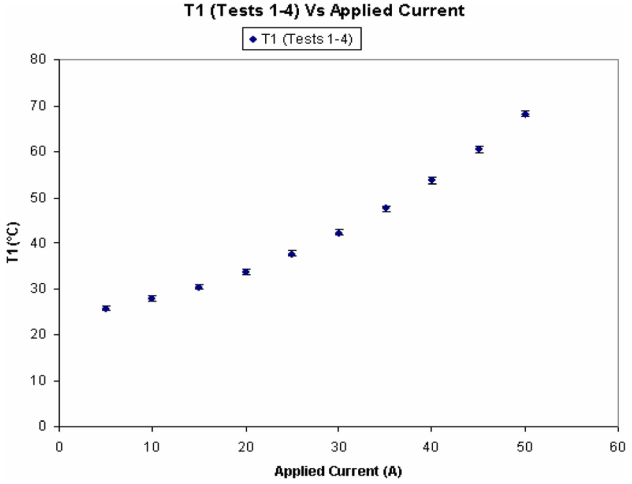

Fig. 23 Connector temperatures at base (T1) versus constant current in the 35A connector (with error bars for all four tests)

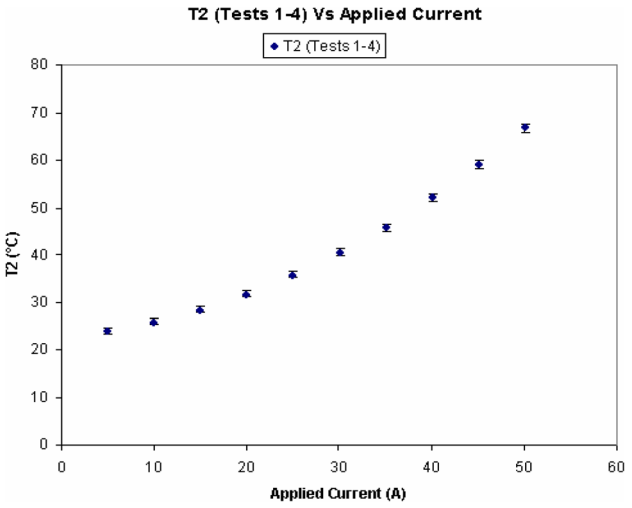

Fig. 24 Connector temperatures at side (T2) versus constant current in the 35A connector (with error bars for all four tests)

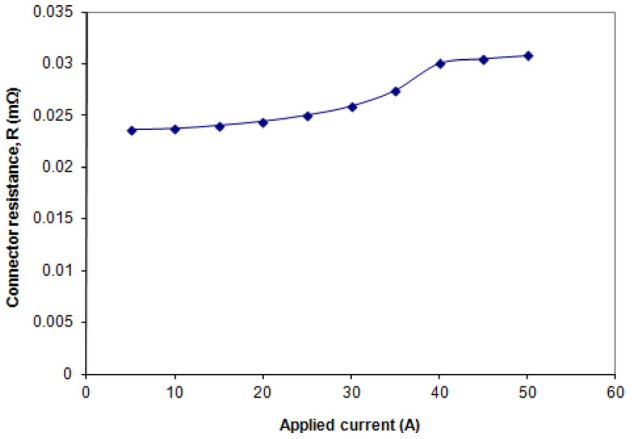

Fig. 25 Plot of connector resistance versus applied current from 35A connector model

0.0033% accuracy. Temperature is measured by K-type thermocouples and signal conditioning.

Experimental tests were conducted for four single 35A connectors by increasing current from 5 to 50 A in steps of 5 A. Therefore, the connector is tested for the same applied currents that are applied in the 35A connector multiphysics model. During the testing, the applied current was held constant for 30 min at each step value (for example, 35 A) so that a steady-state temperature is reached. After that, data are recorded before the next applied current. The voltage drop and temperatures at two locations are measured, as shown in Fig. 21.

In Fig. 22, the measured connector resistance is plotted versus applied currents. The value of nominal connector resistance provided by the manufacturer is 0.24 mΩ. From experimental testing at Auburn, the connector resistance (R) is 0.227 mΩ for an applied current of 35 A. It is reassuring that this value compares very well with that provided by the manufacturer.

An increasing trend of connector resistance versus constant currents is noticed in Fig. 22. It is assumed that the increase of current causes more Joule heating and then shrinks the area of

contact so the connector resistance increases accordingly. It could also be due to expansion causing the current to travel further through the connector, therefore increasing the resistance.

The plots of connector temperatures at base (T1) and at side (T2) are shown in Figs. 23 and 24, respectively. Notice that, expectedly, T1 and T2 increase in a nonlinear way with applied current for all four tests. Very little difference between T1 and T2 is found. This demonstrates that the temperature gradient across the connector is small and that the heating is mostly due to the cables.

In Figs. 22–24, the connector resistance (R), connector temperature at base (T1) and connector temperature at side (T2) data are averaged among four tests and error bars are used to present the standard errors.

Experimental test results for connector resistance (R) are compared with that obtained from multiphysics modeling of the 35A connector. Figure 22 shows the variation of connector resistance with the applied current during experimental testing of four 35A connectors. Figure 25 shows the variation of connector resistance with the applied current (I) in the 35A connector model. In both the figures, an increasing trend (that is, an increase in R with an increase in applied current) was noticed. However, even though the R versus I trend is the same, the values of R obtained from the 35A connector model and experiment are different by an order of 10. This difference can be attributed to the fact that the 35A connector model is only a 2D one and that the amount of bulk resistance between the model and experiment will be different due to the placement of the voltage wires to measure the voltage across the 35A connector.

5 Analysis of Temperature Rises (ΔT, Change in Temperature) in the Cable and Connector

As discussed earlier, it was noticed that the temperature rise (ΔT) in the connector from the 35A connector model (multiphysics FEM model) was very low and therefore theorized that the heating was mostly coming from the cables. To prove this we have derived simple analytical predictions of ΔT (change in temperature) for the connector and also performed some simple experiments to verify them. First, we will show the derivation of these analytical predictions.

The 1D heat conduction equation (that is, Fourier's law) is given as follows [32]:

$$q''_x = -k\, dT/dx \tag{6}$$

where q''_x is the heat flux (W/mm^2), k is thermal conductivity (W/mm K), and dT/dx is the temperature gradient along the x direction. In addition, the following relationships are used:

$$q''_x = q/A \tag{7}$$

$$A = \pi\, r^2 \tag{8}$$

where q is the heat transfer rate (W), A is the cross sectional area of the circular bar (mm^2), and r is the radius of the bar (mm).

Also, we must consider the heating due to electrical conduction (Joule heating) that is given by

$$q = I^2 R \tag{9}$$

where I is the electric current (A) and R is the resistance (Ω).

Resistance for a conductor with a constant cross section and assuming uniform current flow is given by

$$R = (\rho\, x)/A \tag{10}$$

where ρ is the electrical resistivity (Ω mm) and x is the length of the conductor (mm).

By substituting Eq. (10) into Eq. (9), we obtain

$$q = (I^2 \rho\, x)/A \tag{11}$$

Then, by substituting Eq. (11) into Eq. (7), we obtain

$$q''_x = (I^2\, \rho\, x)/A^2 \tag{12}$$

Equation (6) can then be rewritten as

$$\Delta T = \int_{T_1}^{T_2} dT = -\int_0^{L/2} (q''_x/k)dx \tag{13}$$

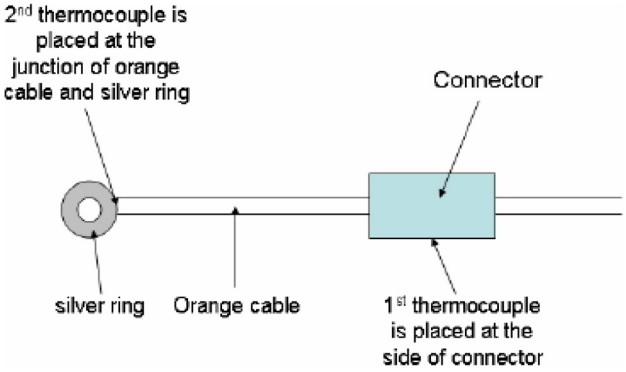

Fig. 26 Schematic diagram of thermocouple placement on cable and connector

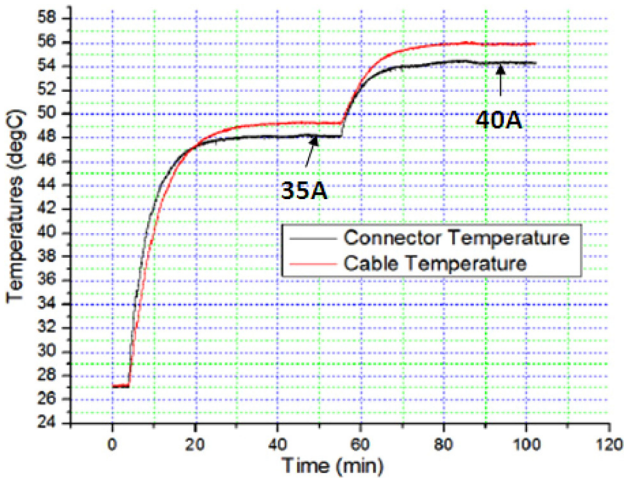

Fig. 27 Experimental variation of cable temperature and connector temperature with time for a 35A connector at 35 A and 40 A applied currents

Table 2 Experimental measurements of cable and connector temperatures and ΔT at two different applied currents

Applied current (A)	Temperature of cable (°C)	Temperature of connector (°C)	Room temperature (°C)	ΔT (for cable) (°C)	ΔT (for connector) (°C)
35	49.26	48.16	25	24.26	23.16
40	55.95	54.33	25	30.95	29.33

And finally, on substituting Eq. (12) into Eq. (13) and on solving the Eq. (13) for ΔT, we obtain the simple analytical prediction

$$\Delta T = -\frac{(I^2 \rho L^2)}{(8A^2 k)} \tag{14}$$

where ΔT is the change in temperature and L is the length of the connector.

Again, for simplicity, the connector cross section is considered as a solid circular bar even though its actual cross section is noncircular and not solid. The values of ρ and k for the connector are given in Table 1. In the analytical model, the following values were used to model the connector: $r = 1.5$ mm, the total length of the connector = 30 mm. For 35 A, the value of ΔT calculated using Eq. (14) is 0.18 °C. Thus, the ΔT across the connector itself is predicted to be extremely small.

In addition to the analytical model, experimental measurements of the temperatures of both the cable and the connector on a single 35A connector have been performed. Figure 26 shows the schematic diagram of the placement of thermocouples to measure cable temperature and connector temperature. Figure 27 shows the experimental variation of cable temperature and connector temperature as a function of time for a 35A connector at two different applied currents of 35 A and 40 A. The change in temperature of the cable and the connector was read after the values had sufficient time to reach a near steady-state value. The values of steady-state temperatures of the cable and the connector as well as the ΔT for the cable and the connector for applied currents of 35 A and 40 A are provided in Table 2.

Predictions from the simple analytical model and the experimental measurements both suggest that the connector temperature is governed mostly by the heat generated in the cables. This also verifies the small values of ΔT (for the connector) obtained from the multiphysics finite element model (see Fig. 14), where only the connector (without the cable) is considered.

6 Conclusions

An inclusive multiphysics finite element based model including multiscale rough surface contact of a 35A connector is established that enables faster convergence than previous methods. The model is solved by employing ANSYS™ with only the need for an external code to make initial predictions of ECR and TCR versus contact pressure. It provides predictions of the stresses, displacements (deformations), Joule heat effects, current density, electric potential, and the temperature distributions in the parts of a 35A connector. Also, upon convergence of the solution in the 35A connector model, force balance on the pin terminal is achieved which implies that the entire connector system in ANSYS™ is under equilibrium.

A few prominent findings were made in this investigation. Conduction of current takes place mostly through a very small region in the connector that is usually near the contacting surfaces. This indicates that the connector designs can be optimized for more efficient use of the available conducting material. Maximum Joule heating occurs in the regions where highest current density is seen in the 35A connector. It was also found that the bulk temperature rise is fairly small, even though experimental measurements indicate otherwise. It is therefore believed that a large portion of the temperature rise in actual connectors is due to the Joule heating in the supply cables. An increasing trend, that is, the connector resistance (R) increasing with the rise in applied currents has been obtained in both the 35A connector model and the experimental tests. This new model serves as a comprehensive and effective tool for developing future automotive connector designs and performing an analysis including the coupled mechanical, electrical and thermal fields, and rough surface contact made of different surface finishes and materials.

References

[1] Miller, J. M., 2004, *Propulsion Systems for Hybrid Vehicles* (IEE Power and Energy Series), MPB Books Limited, Bodmin, Cornwall.
[2] Williams, J., 2005, *Engineering Tribology*, Cambridge University Press, New York.
[3] Jackson, R. L., and Kogut, L., 2007, "Electrical Contact Resistance Theory for Anisotropic Conductive Films Considering Electron Tunneling and Particle Flattening," IEEE Trans. Compon Packag Technol, **30**(1), pp. 59–66.
[4] Kogut, L., 2005, "Electrical Performance of Contaminated Rough Surfaces in Contact," J. Appl. Phys., **97**(10), 103723.
[5] Kogut, L., and Komvopoulos, K., 2005, "Analytical Current-Voltage Relationships for Electron Tunneling Across Rough Interfaces," J. Appl. Phys., **97**(7), 073701.
[6] Greenwood, J. A., and Williamson, J. B. P., 1966, "Contact of Nominally Flat Surfaces," Proc. R. Soc. London, Ser. A, **295**(1442), pp. 300–319.
[7] Chang, W. R., Etsion, I., and Bogy, D. B., 1987, "An Elastic-Plastic Model for the Contact of Rough Surfaces," ASME J. Tribol., **109**(2), pp. 257–263.
[8] Jackson, R. L., 2006, "The Effect of Scale Dependant Hardness on Elasto-Plastic Asperity Contact Between Rough Surfaces," STLE Tribol. Trans., **49**(2), pp. 135–150.
[9] Jackson, R. L., and Green, I., 2006, "A Statistical Model of Elasto-Plastic Asperity Contact Between Rough Surfaces," Tribol. Int., **39**(9), pp. 906–914.
[10] Kogut, L., and Etsion, I., 2003, "A Finite Element Based Elastic-Plastic Model for the Contact of Rough Surfaces," STLE Tribol. Trans., **46**(3), pp. 383–390.
[11] Majumdar, A., and Bhushan, B., 1991, "Fractal Model of Elastic-Plastic Contact Between Rough Surfaces," ASME J. Tribol., **113**(1), pp. 1–11.
[12] Kogut, L., and Komvopoulos, K., 2003, "Electrical Contact Resistance Theory for Conductive Rough Surfaces," J. Appl. Phys., **94**(5), pp. 3153–3162.
[13] Ciavarella, M., Murolo, G., Demelio, G., and Barber, J. R., 2004, "Elastic Contact Stiffness and Contact Resistance for the Weierstrass Profile," J. Mech. Phys. Solids, **52**(6), pp. 1247–1265.
[14] Ganti, S., and Bhushan, B., 1995, "Generalized Fractal Analysis and Its Applications to Engineering Surfaces," Wear, **180**(1-2), pp. 17–34.
[15] Kogut, L., and Jackson, R. L., 2006, "A Comparison of Contact Modeling Utilizing Statistical and Fractal Approaches," ASME J. Tribol., **128**(1), pp. 213–217.
[16] Bora, C. K., Flater, E. E., Street, M. D., Redmond, J. M., Starr, M. J., Carpick, R. W., and Plesha, M. E., 2005, "Multiscale Roughness and Modeling of MEMS Interfaces," Tribol. Lett., **19**(1), pp. 37–48.
[17] Ciavarella, M., Demelio, G., Barber, J. R., and Jang, Y. H., 2000, "Linear Elastic Contact of the Weierstrass Profile," Proc. R. Soc. London, Ser. A, **456**(1994), pp. 387–405.
[18] Jackson, R. L., and Streator, J. L., 2006, "A Multiscale Model for Contact Between Rough Surfaces," Wear, **261**(11-12), pp. 1337–1347.
[19] Kogut, L., and Etsion, I., 2000, "Electrical Conductivity and Friction Force Estimation in Compliant Electrical Connectors," Tribol. Trans., **43**(4), pp. 816–822.
[20] Jackson, R. L., 2010, "An Analytical Solution to an Archard-Type Fractal Rough Surface Contact Model," STLE Tribol. Trans., **53**(4), pp. 543–553.
[21] Wilson, W. E., Angadi, S. V., and Jackson, R. L., 2010, "Surface Separation and Contact Resistance Considering Sinusoidal Elastic-Plastic Multi-Scale Rough Surface Contact," Wear, **268**(1-2), pp. 190–201.
[22] Archard, J. F., 1957, "Elastic Deformation and the Laws of Friction," Proc. R. Soc. London Ser. A, **243**(1233), pp. 190–205.
[23] Ciavarella, M., and Demelio, G., 2001, "Elastic Multiscale Contact of Rough Surfaces: Archard's Model Revisited and Comparisons With Modern Fractal Models," ASME J. Appl. Mech., **68**(3), pp. 496–498.
[24] Persson, B. N. J., 2001, "Elastoplastic Contact Between Randomly Rough Surfaces," Phys. Rev. Lett., **87**(11), 116101.
[25] Angadi, S. V., Wilson, W. E., Jackson, R. L., Flowers, G. T., and Rickett, B. I., 2008, "A Multi-Physics Finite Element Model of an Electrical Connector Considering Rough Surface Contact," *Proceedings of the 54th IEEE Holm Conference on Electrical Contacts*, Orlando, FL, pp. 168–177.
[26] Bryant, M. D., 1993, "Resistance Buildup in Electrical Connectors Due to Fretting Corrosion of Rough Surfaces," *Proceedings of the 39th IEEE Holm Conference on Electrical Contacts*, Pittsburgh, PA, pp. 178–190.
[27] Ossart, F., Noel, S., Alamarguy, D., Correia, S., and Gendre, P., 2007, "Multilayer Contacts in Electrical Connectors: Experimental Results and Modelling," WIT Trans. Eng. Sci., **55**, pp. 89–98.
[28] Swingler, J., and Mcbride, J. W., 2002, "Fretting Corrosion and the Reliability of Multicontact Connector Terminals," IEEE Trans. Compon. Packag. Technol., **25**(4), pp. 670–676.
[29] Wilson, W. E., Angadi, S. V., and Jackson, R. L., 2008, "Electrical Contact Resistance Considering Multi-Scale Roughness," *Proceedings of the 54th IEEE Holm Conference on Electrical Contacts*, Orlando, FL, pp. 190–197.
[30] Angadi, S. V., Jackson, R. L., Choe, S.-Y., Flowers, G. T., Suhling, J. C., Chang, Y.-K., and Ham, J.-K., 2009, "Reliability and Life Study of Hydraulic Solenoid Valve—Part 1—a Multi-Physics Finite Element Model," Eng. Failure Anal., **16**(3), pp. 874–887.
[31] Angadi, S. V., Jackson, R. L., Choe, S.-Y., Flowers, G. T., Suhling, J. C., Chang, Y.-K., Ham, J.-K., and Bae, J.-I., 2009, "Reliability and Life Study of Hydraulic Solenoid Valve—Part 2—Experimental Study," Eng. Failure Anal., **16**(3), pp. 944–963.
[32] Incropera, F., Dewitt, D., Bergman, T., and Lavine, A., 2007, *Fundamentals of Heat and Mass Transfer*, John Wiley & Sons, New Jersey.